

# Universal *versus* Material-Dependent Two-Gap Behaviors in the High- $T_c$ Cuprates: Angle-Resolved Photoemission Study of $\text{La}_{2-x}\text{Sr}_x\text{CuO}_4$

T. Yoshida<sup>1</sup>, M. Hashimoto<sup>1</sup>, S. Ideta<sup>1</sup>, A. Fujimori<sup>1</sup>, K. Tanaka<sup>2</sup>, N. Mannella<sup>2</sup>, Z. Hussain<sup>3</sup>, Z.-X. Shen<sup>2</sup>, M. Kubota<sup>4</sup>, K. Ono<sup>4</sup>, Seiki Komiya<sup>5</sup>, Yoichi Ando<sup>6</sup>, H. Eisaki<sup>7</sup>, S. Uchida<sup>1</sup>

<sup>1</sup>*Department of Physics, University of Tokyo, Bunkyo-ku, Tokyo 113-0033, Japan*

<sup>2</sup>*Department of Applied Physics and Stanford Synchrotron Radiation Laboratory, Stanford University, Stanford, CA 94305*

<sup>3</sup>*Advanced Light Source, Lawrence Berkeley National Lab, Berkeley, CA 94720*

<sup>4</sup>*Photon Factory, Institute of Materials Structure Science, KEK, Tsukuba, Ibaraki 305-0801, Japan*

<sup>5</sup>*Central Research Institute of Electric Power Industry, Komae, Tokyo 201-8511, Japan*

<sup>6</sup>*Institute of Scientific and Industrial Research, Osaka University, Ibaraki, Osaka 567-0047, Japan and*

<sup>7</sup>*National Institute of Advanced Industrial Science and Technology, Tsukuba 305-8568, Japan*

(Dated: October 30, 2018)

We have investigated the doping and temperature dependences of the pseudogap/superconducting gap in the single-layer cuprate  $\text{La}_{2-x}\text{Sr}_x\text{CuO}_4$  by angle-resolved photoemission spectroscopy. The results clearly exhibit two distinct energy and temperature scales, namely, the gap around  $(\pi,0)$  of magnitude  $\Delta^*$  and the gap around the node characterized by the  $d$ -wave order parameter  $\Delta_0$ , like the double-layer cuprate Bi2212. In comparison with Bi2212 having higher  $T_c$ 's,  $\Delta_0$  is smaller, while  $\Delta^*$  and  $T^*$  are similar. This result suggests that  $\Delta^*$  and  $T^*$  are approximately material-independent properties of a single  $\text{CuO}_2$  plane, in contrast the material-dependent  $\Delta_0$ , representing the pairing strength.

PACS numbers: 74.25.Jb, 71.18.+y, 74.72.Dn, 79.60.-i

One of the central issues in the studies of high- $T_c$  cuprates is whether the pseudogap is related to the superconductivity or a distinct phenomenon from superconductivity. In the former scenario, a possible origin of the pseudogap is preformed Cooper pairs lacking phase coherence [1]. In the latter scenario, the pseudogap is due to a competing order such as spin density wave, charge density wave,  $d$ -density wave [2], etc. It has been well known that the pseudogap in the antinodal  $\sim (\pi,0)$  region increases with underdoping as observed by angle-resolved photoemission spectroscopy (ARPES) [3] and tunneling spectroscopy [4]. However, the energy gap measured by Andreev reflection [5], penetration depth [6], and Raman experiments in  $B_{2g}$ -geometry [7, 8], which is more directly associated with superconductivity, exhibits opposite trend, that is, the gap decreases with underdoping, suggesting a different origin of the superconducting gap from the antinodal gap.

A recent ARPES study of deeply underdoped  $\text{Bi}_2\text{Sr}_2\text{Ca}_{1-x}\text{Y}_x\text{Cu}_2\text{O}_8$  (Bi2212) has revealed the presence of two distinct energy gaps between the nodal and anti-nodal region [9, 10]. A similar two-gap behavior has been observed in optimally doped single-layer cuprate  $\text{Bi}_2\text{Sr}_2\text{CuO}_{6+\delta}$  (Bi2201) [11, 12] and  $\text{La}_{2-x}\text{Sr}_x\text{CuO}_4$  (LSCO) [13]. Also, a temperature-dependent angle-integrated photoemission study of LSCO has indicated two distinct gap energy scales [14]. On the other hand, attempts have been made to understand the pseudogap within a single  $d$ -wave energy gap [15, 16, 17, 18]. Valla *et al.* [16] have shown that  $\text{La}_{2-x}\text{Ba}_x\text{CuO}_4$  with  $x=1/8$ , where superconductivity is suppressed due to stripe formation, has a gap of simple  $d_{x^2-y^2}$  symmetry without signature of two gap energy scales. From the measure-

ment of Fermi arc length, Kanigel *et al.* [17] has proposed that the  $T=0$  ground state of the pseudogap state is a nodal liquid which has a single  $d_{x^2-y^2}$  gap. In such a single gap picture, preformed Cooper pairs are the most likely origin of the pseudogap.

Since the doping and temperature dependences of the energy gap would reveal the entangled two-gap behavior, we have investigated the energy gap of lightly- to optimally-doped LSCO by ARPES as a function of doping and temperature. In the present work, the momentum dependence of the gap clearly exhibits two-gap behavior as in the case of heavily underdoped Bi2212: the pseudogap  $\Delta^*$  in the antinodal region and the  $d$ -wave like gap  $\Delta_0$  around the node. Furthermore, from comparison of the present results with those on Bi2212, we have found that the magnitude of the  $\Delta^*$  and the pseudogap temperature  $T^*$  is not appreciably material-dependent, suggesting that the pseudogap is properties of a single  $\text{CuO}_2$  plane. On the other hand, the magnitude of the  $\Delta_0$ , which is proportional to the superconducting gap, is strongly material-dependent ( $\text{CuO}_2$  layer number-dependent) like  $T_c$ .

High-quality single crystals of LSCO ( $x=0.03, 0.07, 0.15$ ) were grown by the traveling-solvent floating-zone method. The critical temperatures ( $T_c$ 's) of the  $x=0.07, 0.15$  samples were 14 and 39 K, respectively, and the  $x=0.03$  samples were non-superconducting. The ARPES measurements were carried out at BL10.0.1 of Advanced Light Source (ALS) and at BL-28A of Photon Factory (PF) using incident photons of linearly polarized 55.5 eV and circularly polarized 55 eV, respectively. SCIENTA R4000 and SES-2002 analyzer were used at ALS and PF, respectively, with the total energy resolution of  $\sim 20$  meV

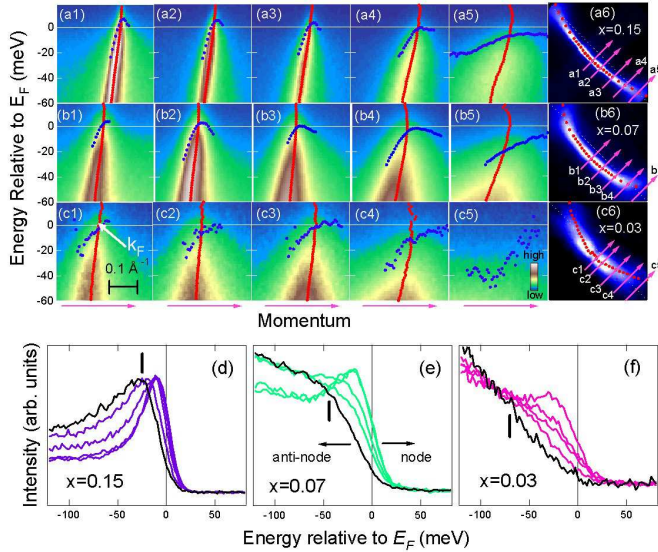


FIG. 1: (Color online) ARPES intensity plot of  $\text{La}_{2-x}\text{Sr}_x\text{CuO}_4$  (LSCO) for cuts across the Fermi surface. (a1)-(a5), (b1)-(b5) and (c1)-(c5): Band image plots in energy-momentum ( $E$ - $k$ ) space for  $x=0.15$ , 0.07 and 0.03, respectively. Energy dispersions determined by MDC's peaks and leading edge midpoints (LEM) are shown by red dots and blue dots, respectively. (a6), (b6) and (c6): Spectral weight mapping at  $E_F$  in momentum space for each doping level. Red dots indicate Fermi momenta  $k_F$  determined by the MDC peak positions at  $E_F$ . White dotted lines indicate the antiferromagnetic Brillouin zone (AFBZ). (d)-(f): EDC's at  $k_F$  for each doping level. Black lines correspond to anti-nodal EDC's and vertical bars represent energy position of the anti-node gap.

and momentum resolution of  $\sim 0.02\pi/a$ , where  $a=3.8 \text{ \AA}$  is the lattice constant. The samples were cleaved *in situ* and measurements were performed from 20 to 155 K. In the measurements at ALS, the electric field vector  $\mathbf{E}$  of the incident photons lies in the  $\text{CuO}_2$  plane, rotated by 45 degrees from the Cu-O bond direction, so that its direction is parallel to the Fermi surface segment around the nodal region. This geometry enhances the dipole matrix elements in this  $\mathbf{k}$  region [19].

In Fig. 1, ARPES intensity in energy-momentum space for various cuts is mapped from the nodal to the anti-nodal directions. The quasi-particle (QP) band dispersions are determined by momentum distribution curve (MDC) peak positions and the Fermi momentum  $k_F$  is defined by the momentum where the QP dispersion crosses the  $E_F$ . The leading edge midpoints (LEM's) of the energy distribution curves (EDC's) are plotted by blue dots around the  $k_F$  for each cut. To quantify the energy gap size, the LEM's at  $k_F$  shall be used in the present analysis. As shown in Fig.1(d)-(f), the LEM's at  $k_F$  are shifted toward higher binding energies in going from the node to the anti-node, indicating an anisotropic gap opening.

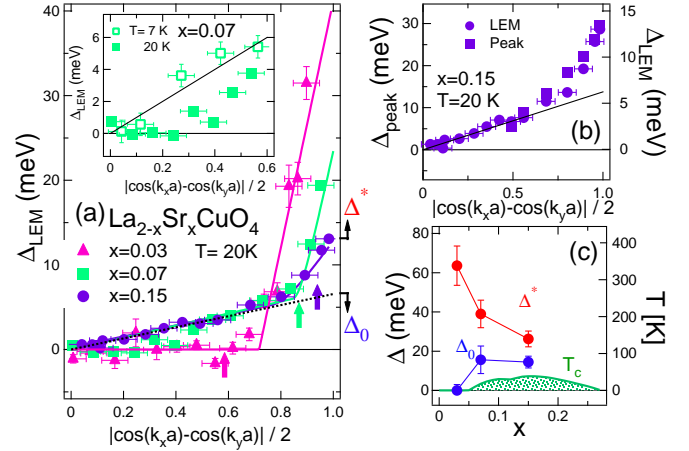


FIG. 2: (Color online) Momentum dependence of the energy gap at  $T = 20 \text{ K}$  in LSCO with various doping levels. (a): Leading edge midpoints (LEM)  $\Delta_{\text{LEM}}$  relative to that at the node. Vertical arrows represent the boundary of the AFBZ. Inset shows LEM near the node for  $x=0.07$  below and above  $T_c (=14 \text{ K})$ . (b): Comparison of the peak position ( $\Delta_{\text{peak}}$ ) and  $\Delta_{\text{LEM}}$  for  $x=0.15$ , indicating the relationship  $\Delta_{\text{peak}} \simeq 2.2\Delta_{\text{LEM}}$ . (c): Doping dependence of  $\Delta^*$  and  $\Delta_0$  obtained by assuming the relation in panel (b).

The gap sizes have been evaluated from the shift ( $\Delta_{\text{LEM}}$ ) of the LEM of EDC's relative to the node. The angular dependence of the gap for each doping is plotted as a function of the  $d$ -wave parameter  $|\cos(k_x a) - \cos(k_y a)|/2$  in Fig. 2(a). These plots do not obey the simple straight line expected for the pure  $d$ -wave order parameter but has a kink at  $|\cos(k_x a) - \cos(k_y a)|/2 \simeq 0.7-0.9$ . Interestingly, the kink occurs near the antiferromagnetic Brillouin-zone boundary but not exactly on it, as shown by vertical arrows. Qualitatively the same results have been obtained for the single-layer cuprates Bi2201 [11] and underdoped Bi2212 [9, 10]. Note that the gaps for  $x=0.07$  near the node are almost closed above  $T_c (=14 \text{ K})$ , but  $d$ -wave like gap opens below  $T_c$  as shown in the inset.

In order to discuss the character of the energy gaps, we define two distinct energy scales  $\Delta^*$  and  $\Delta_0$ :  $\Delta^*$  from  $\Delta_{\text{LEM}}$  closest to  $|\cos(k_x a) - \cos(k_y a)|/2=1$  and  $\Delta_0$  from the extrapolation of the linear dependence near the node ( $|\cos(k_x a) - \cos(k_y a)|/2 \sim 0$ ) toward  $|\cos(k_x a) - \cos(k_y a)|/2=1$ , as indicated in panel (a). Since the  $\Delta_{\text{LEM}}$  is affected by the width of EDC's, the gap magnitude ( $\Delta$ ) is approximately given by 2-3 times  $\Delta_{\text{LEM}}$  [11]. As shown in Fig. 2(b), a relationship  $\Delta = 2.2\Delta_{\text{LEM}}$  well explains both the LEM and peak shift in the  $x=0.15$  data and also explains the data for  $x=0.03$  and 0.07. Therefore, we have assumed this relationship for analysis of the  $\Delta^*$  and  $\Delta_0$  as described below.

In Fig. 2(c), the doping dependence of the observed  $\Delta^*$  and  $\Delta_0$  thus deduced are summarized. The doping de-

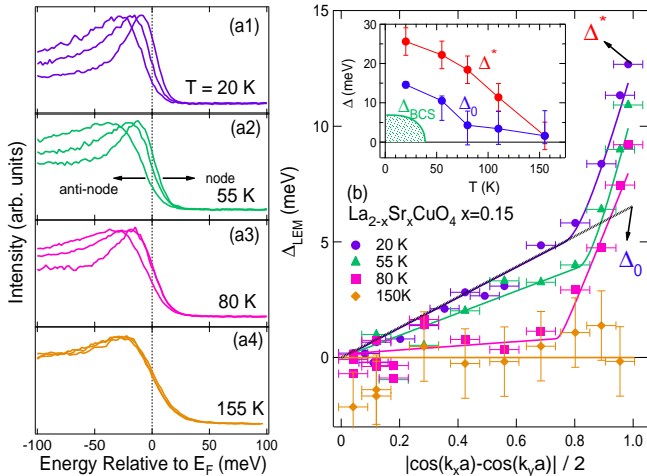


FIG. 3: (Color online) Momentum dependence of the energy gap for  $x=0.15$  at various temperatures. (a1)-(a4): EDC's at  $k_F$  in the nodal to the anti-nodal directions. (b): Momentum dependence of  $\Delta_{LEM}$  along the Fermi surface for  $x=0.15$  at various temperatures. Inset shows the temperature dependence of  $\Delta^*$  and  $\Delta_0$  with the assumption  $\Delta = 2.2\Delta_{LEM}$  as in Fig. 2. The  $d$ -wave BCS gap  $\Delta_{BCS}(=4.3k_B T_c/2)$  is also plotted for comparison.

pendence of  $\Delta^*$  is quantitatively consistent with various spectroscopic data such as  $B_{1g}$ -geometry Raman scattering [8].  $\Delta^* \sim 30$  meV for the  $x=0.15$  sample is consistent with the previous ARPES results, too [13]. On the other hand,  $\Delta_0$  remains unchanged in going from  $x=0.15$  to  $x=0.07$  and vanishes in the non-superconducting sample  $x=0.03$  [20], similar to the results of the lightly-doped Bi2212 [9]. However, vortex-liquid states suggestive of superconducting states were observed in  $x=0.03$  [21]. The present result  $\Delta_0 \sim 0$  for  $x=0.03$  may be due to the high temperature effects similar to the LEM above  $T_c$  near the nodal direction for  $x=0.07$ .

The temperature dependence of the gap is shown in Fig. 3. In Fig. 3(a1)-(a4), EDC's for  $x=0.15$  exhibit clear shifts of the LEM between the nodal and anti-nodal directions in the  $T=20, 55$  and  $80$  K data. In contrast, the LEM at  $T=155$  K show almost no shift between the nodal and anti-nodal direction, indicating that the gap is closed on the entire Fermi surface. The angular dependence of the  $\Delta_{LEM}$  for each temperature are plotted in Fig. 3(b). As shown in the inset,  $\Delta^*$  decreases with increasing temperature and closes at  $T^* \sim 150$  K, again consistent with  $T^*$  obtained from the angle-integrated photoemission results [14].  $\Delta_0$  also decreases with temperature similar to the decrease of  $T_c$ . However  $\Delta_0$  seems finite at  $T=55$  K, slightly above  $T_c$ . Probably, the gap closes near the node direction [18], although the low energy scales in LSCO did not allow us to resolve it.

Now, let us compare the two gap energy scales of LSCO with those of other high- $T_c$  cuprates to clarify their re-

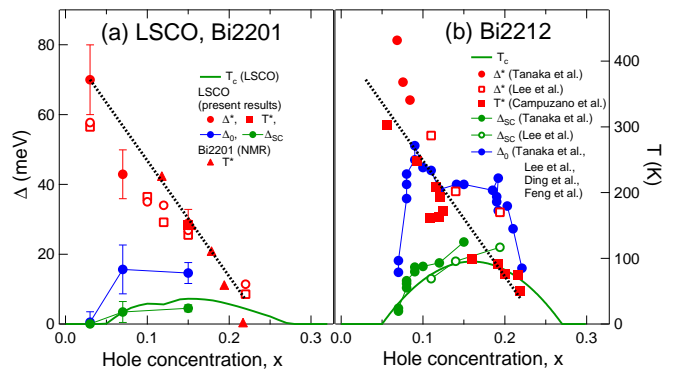


FIG. 4: (Color online) Doping dependence of the characteristic energies ( $\Delta^*$ ,  $\Delta_0$ ) and temperatures ( $T^*$ ,  $T_c$ ) for single-layer cuprates (LSCO, Bi2201) (a) and double-layer cuprates Bi2212 (b). Gap energies  $\Delta$  and temperatures  $T$  have been scaled as  $2\Delta = 4.3k_B T$  in both panels. Parameter values have been taken from NMR results for Bi2201 [30], and ARPES for Bi2212 [3, 9, 10, 31, 32].

lation to  $T_c$ . In Fig. 4(a), the doping dependences of  $\Delta^*$ ,  $\Delta_0$  and  $T^*$  for LSCO and another single-layer cuprate Bi2201 are plotted. In the same manner, those for double-layer Bi2212 which has about twice higher  $T_c$  than those of LSCO are plotted in Fig. 4(b). Interestingly, the doping dependences of  $\Delta^*$  of all these samples approximately scale with  $T^*$  following the relationship  $2\Delta^*/k_B T^* = 4.3$ , reminiscent of the  $d$ -wave BCS relationship [22]. Furthermore, these data fall on approximately the same lines for all the compounds irrespective of the different  $T_c$  as indicated in Fig 4(a) and (b). Especially, pseudogap temperatures for optimally doped  $\text{Bi}_2\text{Sr}_2\text{Ca}_2\text{Cu}_3\text{O}_{10}$  (Bi2223) [23] and Bi2201 [11] are both  $T^* \sim 150$  K, similar to the present result of LSCO  $T^* \sim 140$  K, although they have very different  $T_c$ 's. Therefore, we speculate that  $\Delta^*$  is an universal property of a single  $\text{CuO}_2$  plane and is not much affected by its chemical environment [24]. One possible explanation for the material independence of  $\Delta^*$  is that its magnitude is determined by  $J$ , since the exchange interaction  $J$  is almost material independent. A pseudogap originated from antiferromagnetic spin fluctuations [25] or RVB-type spin singlet formation [26] has its origin in  $J$ .

In contrast to  $\Delta^*$ , the  $d$ -wave order parameter  $\Delta_0$  of Bi2212 is twice as large as those of LSCO, reminiscent of the difference in the magnitude of  $T_c$ . The strong material dependences of  $\Delta_0$  mean that  $\Delta_0$  is not a property only of a single  $\text{CuO}_2$  plane but also influenced by the environment such as the apical oxygens or the block layers and/or the neighboring  $\text{CuO}_2$  planes in multilayer cuprates. Namely, the number of  $\text{CuO}_2$  layers and the distance of the apical oxygen atoms (in block layers) from the  $\text{CuO}_2$  plane are important factors for the supercon-

ducting gap and hence  $T_c$ . Within the model Hamiltonian description of the high- $T_c$  cuprates, the effect from outside the  $\text{CuO}_2$  plane has been modelled using the distant-neighbor hopping parameters  $t'$  and  $t''$  [27], which are affected by the  $p_z$  orbital of the apical oxygen and the position of the empty Cu 4s orbital and characterize the details of band dispersions. In other words, the  $(\pi,0)$  pseudogap does not depend on details of the band structure nor on the parameters  $t'$ ,  $t''$ , but only on  $t$  and/or  $J$ .

If the pseudogap in the anti-nodal region precludes contribution to the superconductivity and the superconductivity comes mainly from the near-nodal region in the underdoped cuprates, the “effective” superconducting gap  $\Delta_{sc} \propto (\text{Fermi arc length}) \times \Delta_0$  rather than  $\Delta_0$  would be more directly related to  $T_c$  [28]. Here, the Fermi arc is defined by the momentum region where the energy gap closes just above  $T_c$ . According to the high-resolution ARPES, the arc length for LSCO ( $x=0.15$ ) is  $\sim 30\%$  of the entire Fermi surface [13], which is consistent with the present results with  $T=80$  K. For  $x=0.07$ , the arc length is  $\sim 20\%$  as seen in the inset of Fig. 2. Using these value for LSCO, the doping dependence of  $\Delta_{sc} = (\text{arc length}) \times \Delta_0$  is plotted in Fig. 4 (a). In the same manner,  $\Delta_{sc}$  for Bi2212 were determined by using the arc length reported in Ref. [10] [Fig. 4(b)]. The plotted  $\Delta_{sc}$  approximately agree with the dome of  $T_c$  through the BCS formula  $2\Delta_{sc}=4.3k_B T_c$ . Particularly, the decrease of  $T_c$  with underdoping can be ascribed to the reduction of the Fermi arc length together with the  $\Delta_0$ , which remains nearly constant till  $x \sim 0.07$  and then drops. As for the non-superconducting  $x=0.03$  sample, the arc length may be too short to produce sufficient carriers for superconductivity or the nodal spectra may have a small gap due to localization as seen in the transport properties [29].

In summary, we have performed an ARPES study of LSCO to investigate the momentum, doping and temperature dependences of the energy gap from the lightly-doped to optimally doped regions. We have clearly shown a signature of the two distinct energy gap scales,  $\Delta^*$  and  $\Delta_0$ . From comparison of the present results with those of other cuprates, we have found that the magnitude of  $\Delta^*$  is almost material-independent, suggesting that the pseudogap is a distinct phenomenon from superconductivity. On the other hand,  $\Delta_0$  exhibits a large difference between materials, reflecting the different superconducting properties including the different  $T_c$ 's. Using the obtained two-gap parameters in conjunction with the Fermi arc picture [28], we have obtained the magnitude of the “effective” superconducting gap in the underdoped region and consistently explained the doping dependence of  $T_c$  in LSCO as well as in Bi2212. The present results enforce the picture of superconductivity on the Fermi arc and clarify how  $T_c$  disappears in the underdoped region. Since the observed material dependence of  $\Delta_0$  is a crucial factor for the high- $T_c$  superconductivity, the relationship

between  $\Delta_0$  and other model parameters such as  $t'$  and  $t''$ , the number of  $\text{CuO}_2$  planes, the apical oxygen - Cu distance, and possibly electron-phonon coupling, has to be clarified in future studies.

We are grateful to C. M. Ho, M. Ido, G.-q. Zheng and C. Panagopoulos for enlightening discussions. This work was supported by a Grant-in-Aid for Scientific Research in Priority Area “Invention of Anomalous Quantum Materials”, Grant-in-Aid for Young Scientists from the Ministry of Education, Science, Culture, Sports and Technology and the USDOE contract DE-FG03-01ER45876 and DE-AC03-76SF00098. Y.A. was supported by KAKENHI 19674002 and 20030004. ALS is operated by the Department of Energy’s Office of Basic Energy Science, Division of Materials Science. Experiment at Photon Factory was approved by the Photon Factory Program Advisory Committee (Proposal No. 2006S2-001).

- 
- [1] J. V. Emery and S. A. Kivelson, *Nature* **374**, 434 (1998).
  - [2] S. Chakravarty, R. B. Laughlin, Dirk K. Morr, and C. Nayak, *Phys. Rev. B* **63**, 094503 (2001).
  - [3] J. C. Campuzano *et al.*, *Phys. Rev. Lett.* **83**, 3709 (1999).
  - [4] N. Miyakawa *et al.*, *Phys. Rev. Lett.* **80**, 157 (1998).
  - [5] G. Deustcher, *Nature* **397**, 410 (1999).
  - [6] C. Panagopoulos, J. R. Cooper, and T. Xiang, *Phys. Rev. B* **57**, 13422 (1998).
  - [7] M. Opel *et al.*, *Phys. Rev. B* **61**, 9752 (2000).
  - [8] M. Le Tacon *et al.*, *Nature Physics* **2**, 537 (2006).
  - [9] K. Tanaka *et al.*, *Science* **314**, 1910 (2006).
  - [10] W. S. Lee *et al.*, *Nature* **450**, 81 (2007).
  - [11] T. Kondo *et al.*, *Phys. Rev. Lett.* **98**, 267004 (2007).
  - [12] M. Hashimoto *et al.*, arXiv:0807.1779 .
  - [13] K. Terashima *et al.*, *Phys. Rev. Lett.* **99**, 017003 (2007).
  - [14] M. Hashimoto *et al.*, *Phys. Rev. B* **75**, 140503(R) (2007).
  - [15] M. R. Norman *et al.*, *Phys. Rev. B* **76**, 174501 (2007).
  - [16] T. Valla *et al.*, *Science* **314**, 1914 (2006).
  - [17] A. Kanigel *et al.*, *Nature Physics* **2**, 447 (2006).
  - [18] J. Meng *et al.*, arXiv:0808.0806 .
  - [19] T. Yoshida *et al.*, *Phys. Rev. B* **63**, 220501(R) (2001).
  - [20] For  $x=0.03$ , although  $\Delta_{LEM} \sim 0$  on most of the Fermi surface, spectral weight is appreciable only near the node, yielding the short Fermi arc.
  - [21] L. Li *et al.*, *Nature Physics* **3**, 311 (2007).
  - [22] H. Won and K. Maki, *Phys. Rev. B* **49**, 1397 (1994).
  - [23] T. Sato *et al.*, *Phys. Rev. Lett.* **89**, 067005 (2002).
  - [24] Disorder has been shown to influence  $T^*$  to some extent. [Okada *et al* arXiv:0709.0220 and arXiv:0704.1698]. .
  - [25] P. Prelovsek and A. Ramsak, *Phys. Rev. B* **65**, 174529 (2002).
  - [26] H. Fukuyama and H. Kohno, in *Physics and Chemistry of Transition-Metal Oxides*, edited by H. Fukuyama and N. Nagaosa (Springer, Berlin, 1999), p. 231.
  - [27] E. Pavarini *et al.*, *Phys. Rev. Lett.* **87**, 047003 (2001).
  - [28] M. Oda, R. M. Dipasupil, N. Momono, and M. Ido, *J. Phys. Soc. Jpn.* **69**, 983 (2000).
  - [29] Y. Ando *et al.*, *Phys. Rev. Lett.* **87**, 017001 (2001).
  - [30] G. q. Zheng *et al.*, *Phys. Rev. Lett.* **94**, 047006 (2005).
  - [31] H. Ding *et al.*, *Phys. Rev. Lett.* **87**, 227001 (2001).

[32] D. L. Feng *et al.*, Phys. Rev. Lett. **86**, 5550 (2001).